PCCP

Accepted Manuscript

ROYAL SOCIETY OF CHEMISTRY

www.rsc.org/pccp

PCCP

ARTICLE

LiCl solvation in N-Methyl-Acetamide (*NMA*) as a model for understanding of Li+ binding to amide plane

Received 00th January 20xx,
Accepted 00th January 20xx

DOI: 10.1039/x0xx00000x

www.rsc.org/

Nikolai Manin[a]‡, Mauricio C. da Silva[b,d]‡, Igor Zdravkovic[b,c]‡, Olga Eliseeva[a] , Alexei Dyshin[a] , Orhan Yaşar[b,c], Dennis R. Salahub[b,d], Arkadiy M. Kolker[a], Michael G. Kiselev[a] and Sergei Yu. Noskov[b,c].

The thermodynamics of ion solvation in non-aqueous solvents remains of great significance for understanding cellular transport and ion homeostasis, design of novel ion-selective materials and applications in molecular pharmacology. Molecular simulations are playing pivotal roles in connecting experimental measurements to the microscopic structures of liquids. One of the most useful and versatile mimetic systems for understanding biological ion transport is N-methyl-acetamide (NMA). A plethora of theoretical studies for ion solvation in NMA appeared recently, but further progress is limited by two factors. One is an apparent lack of experimental data on solubility and thermodynamics of solvation for a broad panel of 1:1 salts over an appropriate temperature and concentration range. The second concern is more substantial and has to do with the limitations hardwired in additive (fixed charge) approximations used for most of the existing force-fields. In this submission, we report on the experimental evaluation of LiCl solvation in NMA over a broad range of concentrations and temperatures and compare the results with those of MD simulations with several additive and one polarizable force-field (Drude). By comparing our simulations and experimental results to density functional theory computations, we discuss limiting factors in existing potential functions. To evaluate possible implications of explicit and implicit polarizability treatments on ion permeation across biological channels, we performed potential of mean force (PMF) computations for Li^+ transport through a model narrow ion channel with additive and polarizable force-fields.
.

Introduction

Inorganic ions play essential and diverse roles in a variety of cellular processes. They act as secondary biological messengers, are responsible for signal transduction, and partake in catalysis as common enzyme cofactors[1]. Over the last couple of decades computational simulations have been successful in replicating and supporting experimental findings[2-6]. Although another alkali cation, Li^+, is present at very low concentrations under normal physiological conditions, understanding the mechanism for the relative affinity of the Na^+ and Li^+ binding site is of great importance for pharmacoplogy[7-10].

Li^+ was detected in human organs and fetal tissues in the late 19th century, indicating importance of lithium to organism function. However, it took another century before physiological importance of lithium to become evident. Early work was conducted on the rats and goats maintained on a low lithium diet. These subjects had high mortality as well as reproductive and behavioural abnormalities. In humans low lithium intake has been associated with higher rates of suicide, homicide, and drug abuse[11]. Lithium is found at very low concentrations and although one of the more toxic alkali metals the mood stabilizing properties have been known since the nineteenth century. Lithium is found in variable amounts in foods, primarily in grains and vegetables. In some areas significant amount of lithium are found in drinking water. Therefore, human dietary intake of lithium depends on location and the type of foods consumed. The available experimental evidence now appears to be sufficient to accept lithium as an essential nutrient; the average daily Li^+ intake for an adult ranges from 650 to 3100 ug[12]. Resurgence of lithium as a antimanic drug is credited to John Cade, who in 1949 reintroduced lithium to the field of psychiatry[12]. Lithium as a therapeutic drug had been hotly debated for decades and further research is needed to settle this debate. The lithium salts are simple to administer and the benefits are evident, however lack of research has prompted FDA to keep the lithium sidelined as an approved drug[12].

The biochemical mechanisms of action of lithium appear to be complex and inter-connected with the functions of several enzymes, hormones and vitamins. The understanding of mechanisms responsible for apparent Li^+ binding to various Na^+-selective enzymes is yet to be established and molecular simulations are expected to play substantial role in the process. A number of different factors have been proposed to be important for explaining competitive cation binding to proteins. These include partial charge transfer and polarization effects upon ion binding to the site[13, 14], often missing in simulations with additive force-fields.

To date several molecular simulation studies were published focusing on structural, energetic and dynamical properties of Li^+

[a] *G.A. Krestov Institute for Solution Chemistry, Russian Academy of Sciences, Akademicheskaya str, 1, Ivanovo, 153045, Russia, E-mail: mgk@isc-ras.ru*

[b] *Centre for Molecular Simulation, BI-447, University of Calgary,2500 University Drive NW, Calgary, AB, T3A 2T3, Canada. E-mail: snoskov@ucalgary.ca*

[c] *Department of Biological Sciences, University of Calgary,2500 University Drive NW, Calgary, AB, T3A 2T3, Canada*

[d] *Department of Chemistry, University of Calgary, 2500 University Drive NW, Calgary, AB, T2N 1N4, Canada.*

† *Sergei Noskov and Michael Kiselev* are corresponding authors for this manuscript

‡ These authors contributed equally to the project

Electronic Supplementary Information (ESI) available: [details of any supplementary information available should be included here]. See DOI: 10.1039/x0xx00000x

solutions in water, Li^+-protein and Li^+-DNA interactions[2, 15-19]. The need for better Li^+ parameters have been further exacerbated by the recent applications of existing potential parameters to studies of polymer-ionic liquids with potential applications in Li+-batteries[20]. However, as the force-fields for proteins and even lipids get better the need for reliable ion parameters keeps increasing[19].

Organic solvents are often a convenient mimetic of most common amino acid main- and side- chains in chemical composition and properties. NMA is a common mimetic for a protein backbone (amide plane) and its carbonyl oxygens are among the most common coordinating ligands for Na^+ and K^+[21] in protein sites. Li+ is known to compete for these binding sites via yet unknown mechanism[10]. Accordingly, we combined experimental and computational methods to test the transferability of ionic parameters developed for aqueous solvation of model 1:1 electrolyte (LiCl) to studies of LiCl solvation in N-methylacetamide. We used experimental measurements on the solvation thermodynamics to improve additive and polarizable force-fields for the Li^+ ion. The present article is organized as follows. We begin by providing a summary of experimental measurements of LiCl enthalpies of solvation, excess heat capacities and volumetric properties in NMA. Next, we examine the performance of different force-fields in the reproduction of solvation thermodynamics and contrast force-field predictions with density functional theory (DFT) computations. Finally, we provide an interpretation and discussion of the performance of additive and polarizable force-fields for the study of ion transport in the gA system.

Experimental and Computational Methods

Experimental measurements of solvation thermodynamics

NMA was purchased from «Acros Organics» with the content of the basic substance of at least 99%. NMA was further distilled under vacuum after two hours of heating with pre-calcined calcium for cleaning. The details on the experimental setup used for studies of ion solvationt thermodynamics and volumetric properties were reported in a series of previous publications[22-29]. The water content of N-methylacetamide was controlled by amperometric titration. LiCl was calcined for several hours at a temperature of 500 K. After calcination, LiCl was recrystallized from distilled water and dried at 373 K. Final drying was carried out under vacuum. The moisture content was determined by Karl Fisher titration. The water levels in the sample were not exceeding 0.005%. The density of NMA/salt solutions was measured by the densitometer "Anton Paar DMA-500" with a standard error of ± $1x10^{-6}$ g/cm^3 in the temperature range from 308.15 to 328.15 K. The temperature dependence of the solvation thermodynamics was monitored with temperature increments of 5 K. Experimental temperatures are reported within ± 0.01 K. The solutions were prepared gravimetrically on a "Sartorius Genius ME235S" analytical balance with an error of ± $1x10^{-5}$ g

The enthalpy of dissolution and dilution of LiCl in N-methylacetamide was measured with an ampoule-type isoperibolic microcalorimeter connected to a computer data acquisition system: PowerGraph 3.3 Professional with an ADC E24 («L-card», Moscow). An automatic control scheme ensures the accuracy of temperature maintenance up to 6 • 10^{-4} K and the temperature and the thermal sensitivity of the measuring cell calorimeter was 10.4 K and 1 • 10^{-3} joules respectively. The instrument error was 0.6 - 1%. The thermal effect of dilution was corrected in a two-stage protocol. The dilution effects due to the pure solvents were measured by breaking the empty vials and evaporation of the solvent in the void volume ("b" - a large vial, "m" - a small vial): q(T=310 K,b) = 0.0327 cal, q (310K, m) = 0.0403 cal, q (320 K, b) = 0.037 cal, q (320 K, m) = 0.007 cal, q (330 K, b) = -0.002 cal, q (330K, m) = 0.03 cal. Here q is the calorimetric heat. In a second set of experiments, a similar routine was used to determine the heats of dilution of salt solutions: q_1 (310 K) = 0.007 cal, q_1 (320 K) = 0.038 cal, q_1 (330 K) = 0.06 cal. Assessment of the reliability of the calorimeteric measurements and accuracy of the data was verified by measuring the enthalpy of KCl solvation in water (mean of 20 measurements is -4.09 ± 0.036 kcal/mol, consistent with the tabulated value: -4.089 ± 0.018 kcal/ mol)[30, 31]. The enthalpy of dissolution of LiCl in NMA (ΔH^m_{solv}) was calculated using formula (1) with the enthalpies of dilution of concentrated salt solutions of (ΔH^m_{solv}).

$$\Delta H^m_{solv} = \Delta H^{\boldsymbol{m_{final}}}_{solv} - \Delta H^{\boldsymbol{m_{initial}} \rightarrow \boldsymbol{m_{final}}}_{solv} \quad (1)$$

where m_{inital} and m_{final} are starting and ending molal electrolyte concentrations in the solution, respectively. The resulting values from experimental measurements were corrected for the lattice enthalpy of LiCl ($\Delta H_{lattice}$=-204.59 kcal/mol)[32, 33] of LiCL to enable direct comparisons to results of Molecular Dynamics simulations.

QM Computations and force-field optimization

The LiCl-NMA complex formation reactions in gas phase, Eq. (2) and (3), were investigated with the PBE[34], BLYP[35-37], PW91[38], TPSS[39], B3LYP[40, 41], B3PW91, BMK[42] and M06[43] functionals with the 6-311+G(d,p)[44, 45] basis set. The Def2-TZVPD basis set was also used with PBE, TPSS and B3LYP functionals only for LiCl-(NMA) and LiCl-$(NMA)_2$ complexes to check/compare the quality of 6-311+G(d,p) basis set, since Def2-TZVPD contains (3d,1f) extra polarization function to the heavy atoms. A full optimization of the molecular structures was done in Cartesian coordinates with no constrains to the geometries. In the equilibrium molecular structures the hessians were calculated and the harmonic frequencies were obtained. Hence, the main reactional thermodynamic functions ($\Delta_R E$, $\Delta_R U^\theta$, $\Delta_R H^\theta$, $\Delta_R G^\theta$, $\Delta_R S^\theta$) for the LiCl-NMA complexes were calculated. All calculations were done in Gaussian-09 rev. A2 package[46] and the basis set superposition error (BSSE)[47, 48] was corrected to all calculations.

$$Cl^-_{(g)} + x.NMA_{(g)} = Cl(NMA)_x{}^- \qquad x = 1\ to\ 4 \qquad (2)$$

$$Li^+_{(g)} + x.NMA_{(g)} = Li(NMA)_x{}^+ \qquad x = 1\ to\ 4 \qquad (3)$$

To use the information from gas-phase cluster optimization, specific potential parameter sets were chosen for corrections of the existing force-fields for Li^+. For example, for Li^+–NMA interactions, we started by using a dimer structure from DFT calculation with the B3LYP functional. For the dimer, we chose three objective functions $x_{\Delta E}{}^2 = (\Delta E_{QM} - \Delta E_{Model})^2$, $x_r{}^2 = (r_{QM} - r_{Model})^2$, and $x_\theta{}^2 = (\theta_{QM} - \theta_{Model})^2$ to minimize simultaneously in the CHARMM-38 package. ΔE is the Li^+–NMA dimer interaction energy, r is the distance between the cation and the NMA carbonyl oxygen atom, and θ is the intermolecular angle (C═O–Li^+) formed by the carbonyl group and the cation. In subsequent iterations, we searched for the parameter sets minimizing the following function $x_r{}^2 = \Sigma_{i=1}{}^n (r_{i,QM} - r_{i,Model})^2$, in which n indicates the number of NMA molecules in the cluster, and i represents the index of each NMA molecule in the complex.

MD simulations

The system was built in CHARMM by running Monte-Carlo runs placing 665 NMA molecules in a cubic box with dimensions corresponding to the density of bulk NMA. Lithium (Li^+) and chloride (Cl^-) ions were placed in random positions in the box to obtain desired concentrations of 0.05, 0.10, 0.15, 0.20, 0.25, 0.30, 0.35, 0.4, 0.5 and 1 mol/kg. The simulation box was equilibrated for 10ns followed by 50 ns of production run. Each of the runs was performed with different parameters for the Li^+ ion and previously published parameters for Cl^-. All the other parameters were kept constant amongst the three simulation runs. The simulations were then analyzed and the radial distribution function was obtained using VMD. All simulations with additive (CHARMM-27, Cheatham force-field) and polarizable force-fields were performed with cubic Periodic Boundary Conditions in the NPT ensemble. Electrostatic interactions were calculated using particle-mesh Ewald (PME) summation[26] with a coupling parameter of 0.34 and a 6th-order spline for mesh interpolation. Non-bonded pair lists were maintained out to 16 Å, and a real-space cutoff of 12 Å was used with Lennard–Jones (LJ) interactions truncated via an atom-based energy switch algorithm[27] from 10 to 12 Å with long-range energy[28] and pressure[29] LJ corrections applied. The SHAKE algorithm was used to maintain the bond lengths that involve hydrogen atoms.

Table 1: Parameters for Li^+ and Cl^- used for simulations with additive and polarizable force-fields

		q (e)	$R_{min}/2$ (Å)	ε(kcal.mol^{-})	α(Å³)
Li^+	Set 1	+ 1.00	1.2975	-0.00233	
	Set 2	+ 1.00	1.0250	-0.02799	
	Set 3	+ 1.00	1.3325	-0.00233	
	Drude	+ 1.00	1.1000	-0.03000	-0.032
Cl^-	Set 1	- 1.00	2.2700	-0.15000	
	Set 2	- 1.00	2.5130	-0.03559	
	Drude	-1.00	2.4811	-0.07197	-3.69

Set 1 is C27 parameters with previously developed NBFIX values[16], Set 2 is force-field developed by Cheatham and colleagues[18]; Set 3 is adjusted CHARMM-27 parameters; Drude corresponds to the Drude force-field adjusted to reproduce gas-phase QM energetics and interaction energy distributions. q corresponds to ionic charge; α- corresponds to atomic polarizability; ε and R_{min} corresponds to standard parameters of the Lennard-Jones (LJ) interaction potential. The pair-specific parameters E_{min} and R_{min} (referred to as NBFIX in the CHARMM force-field), were used to override the default values determined by the Lorentz–Berthelot combination rule. Set 3 has updated $NBFIX_{O\text{-}Li}$ E_{min} = -0.0098 kcal/mol and R_{min}=2.82 Å; The following off-diagonal NBFIX terms were added to ion parameters (atom types corresponds to Drude CHARMM-36 force-field): Li^+/OD2C1A (Carbonyl oxygen) E_{min} = -0.05 kca/mol and R_{min} = 2.750 Å; Li^+/Lone Pair E_{min}= -0.08 kcal/mol and R_{min} = 2.69 Å; Cl^- /ND2A2 (NMA nitrogen): E_{min} =-0.08 kcal/mol and R_{min} = 4.65 Å Cl^-/HDP1A (polar hydrogen): E_{min} =-0.001 kcal/mol and R_{min} =3.54 Å.

The off-diagonal Lennard-Jones interactions (NBFIX) terms were used to describe interactions between Li^+ and carbonyl oxygens in simulations with Set 1 and Set 3. The corrected force-field reproduces the hydration free energy of Li^+ (target ΔG = -122.36 kcal/mol in TIP3P water[49-51]) and reported structural properties of hydrated Li^+ as well as transport properties. To model electronic polarization effects in the NMA and gramicidin A simulations we employed a polarizable Drude force-field for water, protein and lipids developed by the groups of MacKerell and Roux[29-31]. The positions of auxiliary Drude particles attached only to heavy atoms were propagated via an extended Lagrangian formalism through the assignment of a small mass (0.4 amu) at low temperature (1 K) using a separate thermostat. The Velocity-Verlet (VV2) integrator and the Langevin thermostat[29,31] were used for all simulations involving polarizable models. The simulation time for runs employing the polarizable force-field varied from 15 to 25 ns.

Potential of Mean Force for gA simulations

To test the performance of different force-fields and approximations on energetics of ion transport across biological channels we performed computations of 1D Potential of Mean Force (PMF) across a gramicidin A system. The simulation box includes a gramicidin A (gA) helical dimer [PDB:1JNO][52] embedded in a dimyristoylphosphatidylcholine (DMPC) bilayer. The lipid bilayer contains 20 DMPC molecules, hydrated with 1 M LiCl electrolyte solutions consisting of 19 Li^+ and Cl^- pairs and 1080 water molecules in a hexagonal primary cell. The system was hydrated with 1M of electrolyte to ensure good sampling of the bulk electrolyte. During the simulations used to calculate the single-ion potential of mean force (PMF), W(r), other ions were excluded from a sphere of radius 14 Å defining the pore region, using a repulsive flat-bottom spherical harmonic restraint with force constant 5 kcal/mol. In keeping with the protocol outlined by Allen et al. [53, 54] , we limited the lateral displacement of the ion with a flat-bottom cylindrical restraint with radius 8 Å (relative to the center of mass of the dimer) and force constant 10 kcal/mol/A^2. For Umbrella Sampling calculations, harmonic potentials with force constant 10 kcal/mol/Å^2 were implemented for each of 81 windows, positioned in 0.5 Å increments from $-20 \le z \le 20$˚A. For each window, equilibration was carried out for 200 ps prior to 1.0 ns of trajectory generation for the PMF both for simulations performed with polarizable and non-polarizable force-fields. The resulting biased ion density distribution was symmetrized and the weighted histogram analysis method (WHAM protocol) was used to recover the PMF for ion permeation across the gA channel. It should be noted that there are no developed parameters for C- and N-termini for gramicidin in the Drude force-field. Both formyl- and ethanol-amine capping were replaced by Ala and the following terminal groups were used: Acetylated N-terminus (ACE) and N-Methylamide C-terminus (CT3) to maintain electroneutrality. The *ad-hoc* parameters are expected to affect barriers/binding wells located around the center of the membrane and at the entrance.

Results and Discussion

The studies of ion solvation in aqueous and non-aqueous media is a recurrent topic in modern chemical thermodynamics[55-58]. Numerous research reports presenting MD simulations of ion binding to macromolecules rely on the quality of the force-field. Most of the developed force-fields are calibrated against available experimental data on ion solvation in water with an implicit assumption on the parameter transferability. In many cases, it is a fully justified assumption; however, our prior studies of ion selectivity in membrane proteins led to an introduction of special corrections (NBFIX term in CHARMM-27 force-field) to accurately reproduce ion binding energetics to common functional moieties in proteins[16, 21]. All of the studied force-fields were capable of reproducing the concentration dependence of the density for NMA-LiCl solutions. The

experimental data on the solution density as a function of concentration and temperature is collected in the Supplementary Materials (Table S1 and Figure S1). Below we provide experimental data on the solvation of LiCl in N-methylacetamide, a common mimetic of a protein backbone, therefore providing a unique opportunity to cross-validate the performance of popular force-fields developed on the basis of ion solvation in water. This paper

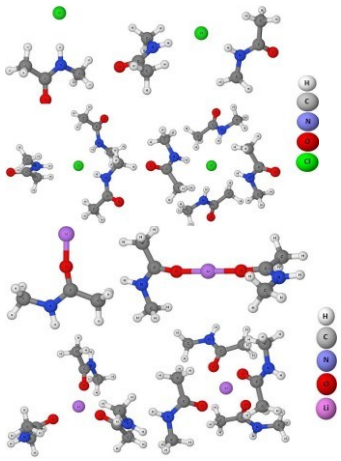

Figure 1: Top: $Cl(NMA)_x^-$ equilibrium molecular geometries in different NMA stoichiometries. **Bottom:** $Li(NMA)_x^+$ equilibrium molecular geometries in different NMA stoichiometries.

focuses specifically on Li^+ solvation since Cl^- solvation in NMA has been investigated in detail in prior reports.

Gas-Phase Energetics and Geometries of NMA-Ion Clusters

To investigate the performance of different force-fields in descriptions of ion-NMA energetics and geometry, we performed a series of DFT calculations on $Li(NMA)_x^+$ and $Cl(NMA)_x^-$ clusters. The characterized molecular equilibrium structures for LiCl(NMA) complexes are summarized in Figure 1 and better presented on supplementary material in Figures S5 to S13. The main characteristic of the equilibrium geometries for ion-NMA complexes, such as molecular bonds and bond angles, are collected in Supplementary Tables S5-S10. Only the bonds CO and NH and the bond angle OCN, CCN and CNC showed some dependence on the choice of the functional judged by the standard deviation (σ) (Table S6). The bi-complexes of $Cl(NMA)_2^-$ displayed an angular/bent geometry. The $Li(NMA)_2^+$ bicomplexes were linear in all characterized equilibrium structures regardless of the chosen functional. The methyl dihedrals are affected by the complexation and different orientations of the methyl dihedrals are shown depending on the ion and the type of complex in Figure 1 and in Figures S5 to S13. The results are in excellent agreement with previous QM studies done on smaller model systems containing hydroxy and carbonyl groups[59]. To re-optimize the interactions of the ion-NMA clusters we examined multiple properties that are relevant to the study of biological binding sites[60]. The properties examined included the interaction energies and the coordination geometries. Tables S11 to S12 list the energetics and some structural parameters computed with *DFT* and force filed calculations to ion-NMA mono/bi-complexes. It was found that the additive force-fields, even corrected, tend to underestimate strongly (~5-7 kcal/mol for Cl^- and >10 kcal/mol for Li^+) interaction energies. This trend is exacerbated for bi-complexes where minimization with the CHARMM-27 and Cheatham force-field parameters resulted in interaction energies of -74.1 kcal/mol and -78.9 kcal/mol, respectively, vs. QM interaction energies ranging from -96.5 to -99.76 depending on the choice of the DFT functional. The introduction of the optimized off-diagonal LJ term (NBFIX) to Set 3 force-field allows for a correct reproduction of gas-phase energetics. The analysis of equilibrium geometries summarized in Tables S8 to S10 also revealed a number of very serious flaws in the performance of the force-fields based entirely on the aqueous solvation data. The minimized geometries for ion-NMA complexes obtained with additive force-fields show significant deviations from ones from QM minimization computations, while adding account for polarization allow to reproduce both gas-phase energetics and geometry of optimized complexes.

Concentration Dependence of LiCl solvation in NMA

Table 2 summarizes experimental data on enthalpies of LiCl solvation in NMA as a function of salt concentration and temperature. The simulated data points are collected in Table 3 and compared to measured enthalpies in Figure 2.

Table 2. Measured solvation enthalpies of LiCl-NMA solutions as a function of concentration and temperature

T=308 °K		T=318 °K		T=328 °K	
m (mol/kg)	**ΔH** (kcal/mol)	**m** (mol/kg)	**ΔH** (kcal/mol)	**m** (mol/kg)	**ΔH** (kcal/mol)
0.00244	-214.11	0.00369	-215.29	0.00268	-216.03
0.00355	-214.13	0.00518	-214.99	0.00707	-215.75
0.00651	-213.59	0.00742	-214.68	0.01071	-215.58
0.01102	-213.70	0.01292	-214.63	0.01268	-215.44
0.01117	-213.56	0.01364	-214.56	0.02023	-215.14
0.01618	-213.41	0.012	-214.19	0.02031	-215.25
0.02197	-213.31	0.02643	-213.78	0.02876	-214.91
0.02438	-213.23	0.02691	-213.91	0.03204	-214.88
0.03032	-212.81	0.03372	-213.71	0.03808	-214.77
0.03868	-212.87	0.0371	-213.97	0.03401	-214.67
0.03877	-213.04	0.04711	-213.89	0.04586	-214.79
0.04763	-212.76	0.06835	-213.67	0.06102	-214.75
0.08382	-212.90	0.07471	-214.01	0.06959	-214.74
0.25458	-217.82	0.11524	-213.97	0.0799	-214.61
0.31142	-219.37	0.16507	-214.78	0.10625	-214.77
		0.23153	-216.57	0.18724	-216.0
				0.31142	-218.68

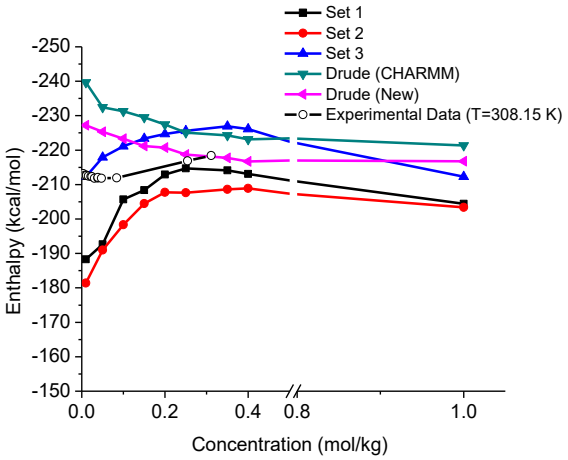

Figure 2. Concentration dependence of LiCl solvation enthalpy in NMA from MD simulations with various models and experimental measurements

All simulations performed with additive force-fields with the exception of Set3, adjusted to match solvation free energies of Li^+ in aqueous solutions, underestimate strongly the solvation enthalpy for the dilute region but display better performance for the concentrated salt solutions. Polarizable force-fields display the opposite trend. Both of the studied sets overestimate solvation thermodynamics in the dilute region and, similarly to the other studied force-fields, display better performance for the concentrated solutions.

Table 3. Concentration dependence of solvation enthalpies of LiCl-NMA solutions for additive and polarizable potential models *

m (mol/kg)	Set 1	Set 2	Set 3	Drude	Drude-NBFIX
0.01	-188.31 (11.1 %)	-181.42 (14.6%)	-212.31 (0.13 %)	-239.69 (12. 7 %)	-227.23 (6.8 %)
0.05	-192.64 (9.06 %)	-190.99 (9.8 %)	-217.92 (2.87 %)	-232.44 (9. 7%)	-225.31 (6.3 %)
0.1	-205.71 (3.0 %)	-198.36 (6.5 %)	-221.12 (4.3 %)	-231.27 (9.05 %)	-223.31 (5.3 %)
0.15	-208.39 (1.7 %)	-204.45 (3.5 %)	-223.34 (5.3 %)	-229.51 (8.3 %)	-221.18 (4.3 %)
0.25	-214.67 (1.1 %)	-207.61 (4.5 %)	-225.61 (3.9 %)	-225.11 (3.4 %)	-218.71 (0.3 %)
0.35	-216.21	-208.61	-226.92	-225.87	-217.71
0.5	-211.21	-207.332	-222.45	-223.413	-217.01
1.0	-204.41	-203.41	-212.31	-221.34	-216.76
Average Error	4	6	3.5	7.5	4

*All enthalpies are reported in kcal/mol. The errors are reported in parenthesis relative to the experimentally measured ΔH^m_{solv})

The experimental enthalpies show a smooth increase from -213 kcal/mol to -218 to 220 kcal/mol in the interval between infinite dilution to m=0.15-0.25 mol/kg. They also show a shallow minimum around m=0.2 mol/kg. It might be noted that the Drude (new) force-field also yields a convex shape, albeit with a displaced minimum, at around 0.4 mol/kg and a much deeper and longer descent.

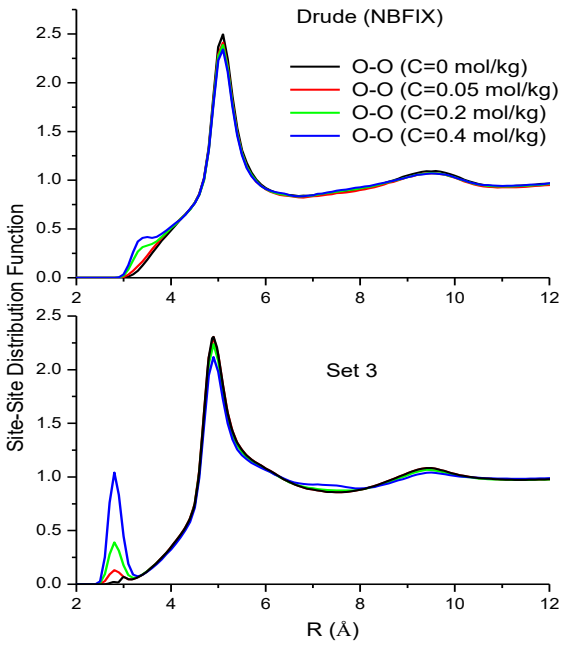

Figure3. Effect of ion concentration on NMA structure. Site-Site radial distribution functions for O-O with the Drude NBFIX-corrected polarizable (top) and Set 3 additive force-fields (bottom) simulations.

Due to solubility limits we were unable to extend our measurements past m=0.35 mol/kg. The introduction of the pair-specific NBFIX corrections (Set 3 and both Drude simulations) into the potential function led to an improved description of the solvation thermodynamics for additive and polarizable force-fields at infinite dilution. The corrected force-fields display average errors of about 3.5 to 4 % vs. 7-8 % in uncorrected force-fields. Given the local concentration of Li^+ in the protein binding sites, polarizable force-fields are expected to perform better at describing ion-protein site interactions. It is important to stress, that we chose to rely on parameterized and tested parameters for Cl^- and this may take a toll on the comparison to experimental data. Clearly, further improvements to the force-fields will be required before fully satisfactory comparisons with experiment can be made throughout the measured concentration range.

Molecular Structures of LiCl solutions in NMA

It has previously been shown that the hydration structure of monovalent salts from the Drude polarizable model closely matches experimental data and *ab initio* results[3, 61-64]. However, most of the prior studies were done in the limit of infinite dilution without much emphasis on the concentration dependence of the solvent structure. Figure 3 shows the radial distribution function (RDF) of the solvent oxygen-oxygen pairs to characterize the effect of LiCl on the NMA structure. The salt effect is even more pronounced on the O-O RDF. An increase in LiCl concentration led to a formation the O-O pairing pre-peak at R=2.9-3.0 and 3.3-3.4 Å for additive and polarizable force-fields, respectively. The appearance of this peak may be explained by the substantial presence of the NMA-Li^+-NMA complexes in addition to the standard dimers. The gas-phase optimization of the geometry for this complex illustrated in Figure 1 and Table S12 show that the geometry of the NMA-Li^+-NMA complex

is almost linear allowing for shorter distances between NMA oxygens. The oxygen-oxygen distance for this complex in a gas phase is R= 3.2 – 3.4 Å. The pure NMA lacks solvent pairing at this distance[21].

An increase in LiCl concentration has relatively modest effect on hydrogen-bonding patterns in NMA (shown in Figure 4) with a progressive decrease in the O-H coordination number from 1.01 in pure NMA to 0.92 in 400 mM LiCl solution (Drude force-field). Set 3 displays a very similar trend. Both force-fields predict the location of the first peak for the O-H RDF (not shown) to be at 2.1 Å and the first minima at 2.9 Å. The ion coordination numbers in liquid NMA were calculated by integrating the Li^+-O and Cl^--N RDFs, up to the outer limit of the first solvation shell (3.2-3.5 Å). The calculated

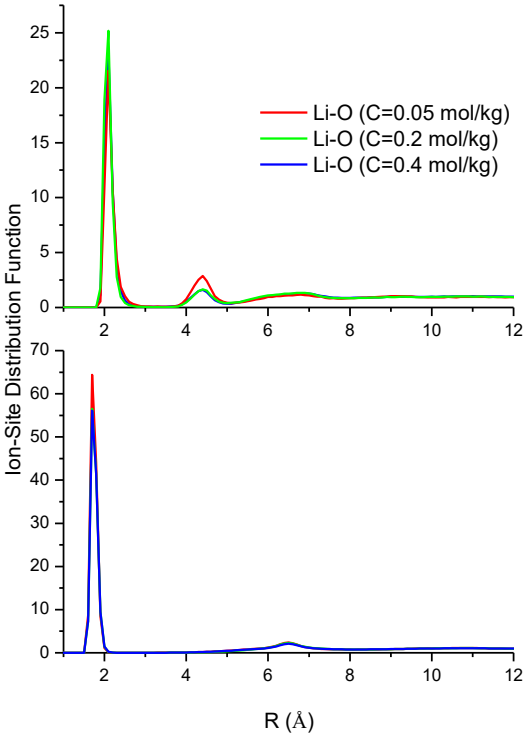

Figure 4. Li^+-Oxygen Distribution Functions. Site-Site distribution functions for Li^+-O with the Drude-NBFIX polarizable (top) and SET 3 additive force-fields (bottom) simulations.

coordination numbers for Li^+ from the polarizable Drude model are 2.81, 2.97 and 3.05 for C=0.05, 0.2 and 0.4 M, respectively. The corresponding values calculated from Set 3 are 3.9, 4.1, and 4.0, respectively. The coordination numbers are considerably smaller with the Drude polarizable force-field than those computed with the additive Set 3. While these results are consistent with numerous studies[14, 15, 65-70] that have considered the effect of induced polarization and previously reported data for Na^+ and K^+ solvation in NMA[21], there are no experimental data available to cross-validate predictions from simulations with polarizable force-fields.

The key difference between RDFs computed with polarizable and non-polarizable force-fields lies in the position of the first peak, which is shifted towards shorter distances in simulations with additive force-field (set 3), and its height. The polarizable force-field predicts an apparent formation of a second solvation shell (R~4.0 Å), the process disrupted by an increase in salt concentration. Ohtaki et al. used X-Ray diffraction[56] to study LiCl solvation in formamide, a solvent chemically close to NMA, found that the average Li-O distance is 2.25 Å, which is very close to that predicted by simulations with the polarizable force-field (2.15 Å). The additive force-field predicts this distance to be much shorter: 1.8-1.9 Å. Recent application of Car-Parrinello *ab-initio* Molecular Dynamics simulations to studies of Li^+ solvation in water, methanol and ethanol[71] also highlighted saddle but important features of ion coordination in aqueous and non-aqueous solvents missing in simulations with additive force-fields. The position of the first peak between Li+ and solvent polar oxygen was changing progressively from 2.0 Å in water to 2.02 Å and 2.04 Å in methanol and ethanol, respectively. Four solvent molecules were found to coordinate solvated Li^+ ion. The authors also noted strong separation between first and second solvation shells, also observed in all simulations reported in this submission. The results suggested that direct account for electronic polarization has a major impact on the simultaneous description of the energetic and structural properties of 1:1 electrolyte solvation in a biomimetic solvent such as NMA. That is expected to have a major effect on the studies of ion binding to proteins.

Additive and Polarizable Simulations of Li^+ binding to the gA channel

To investigate implications of the explicit polarization we have chosen to evaluate the PMF for a single ion transport across a well-studied system – gramicidin A (gA). The gramicidin channel provides a permeation pathway lined up with a backbone carbonyl e.g. NMA-like moieties. The pathway also contains a single-file water wire. Li^+ transport in the gA system is well studied with reported dissociation constants of the order of 100-200 mM[72, 73]. It has been suggested recently that implicit account for polarization has a drastic effect on the shape of the Potential of Mean Force controlling ion transport[74] impacting locations and heights of barriers for an ion transport. Furthermore, there are multiple reports suggesting that lack of explicit polarization is likely to affect the height of the barriers experienced by the permeant ion and therefore would lead to significant underestimation of binding constants and, hence, conductance[53, 54]. The barriers reaching up to 15-20 kcal/mol lead to several orders of magnitude difference from experimentally measured conductance. In keeping with the reported selectivity of gA channels, barriers are higher than those reported for Na^+ and K^+, respectively[75].

Our results with all additive force-fields (Figure 5) display a high barrier located around the middle, inconsistent with experimental data on Li^+ but in keeping with previous simulations with additive force-fields performed for Na^+ and K^+[54, 75]. Interestingly, the PMF computed with Set 3 including corrected NBFIX parameters shows a stabilization of an outer binding site reported to exist in gramicidin based on 2D PMF computations[76]. This trend is missing in all other simulations; however, we considered only 1D PMFs shown in Figure 5. Experimentally, a permeant monovalent cation (K^+) has a stable

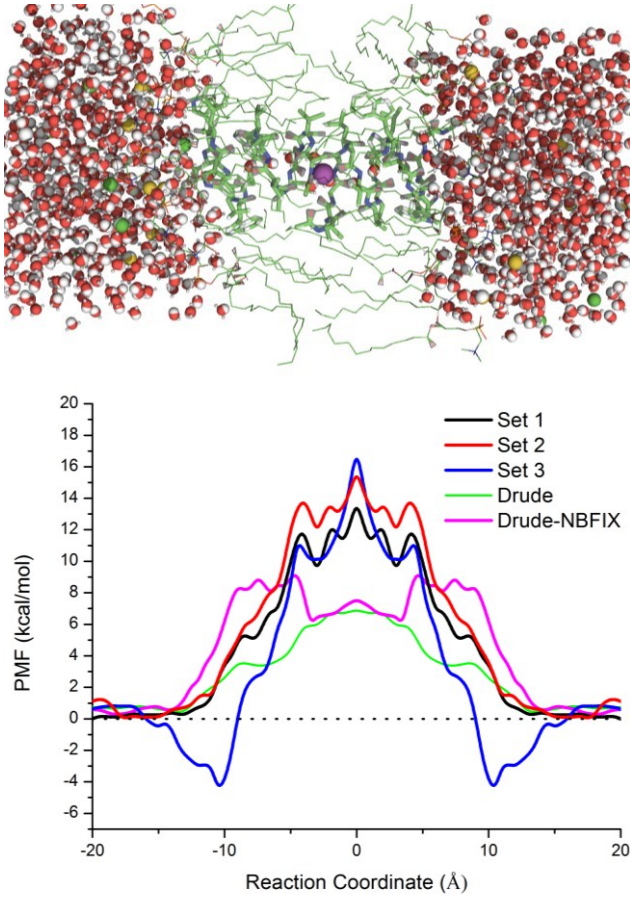

Figure 5. Top panel: Molecular system for studies of Li^+ permeation. gA dimer is shown as sticks. The Li^+ is shown as a purple sphere, while the lipids (DMPC) are schematically shown as lines. Bottom Panel: PMF profiles for additive and polarizable models used in this work

binding site at the outer surface of the protein (10.2 < *z* < 12.5 Å) and the inner site is located between (6.9 < *z* < 12.5 Å)[77].

The Drude-NBFIX PMF displays a shallow binding site at z~ 10 Å and another one at z ~7.5 Å. It also show the formation of a local minimum located around the center of the membrane. Interestingly, prior simulations with the AMBER force-field indicate a propensity for ion binding at this position and so does the GROMOS force-field[75]. The PMF computed with the original Drude force-field also contains two binding sites, but has a barrier at the position equivalent to z=0.0 Å. The simulation run with a polarizable force-field developed in this work shows a significant decrease in the barrier for ion permeation reducing it to 5-7 kcal/mol vs. 10-14 kcal/mol for additive force-fields. The equilibrium dissociation constants for an ion computed by an integration of the PMF in the region from -15 to 15 Å range from 3.5 M for additive force-fields to 370 mM for polarizable ones in better accord with the experimentally measured <200 mM range[72, 73]. It is important to stress that we were unable to observe drastic differences in the PMF shapes between additive and polarizable force-fields reported in Ref. 35. None of our simulations result in a saw-tooth permeation profile obtained with the charge-equilibration polarizable model by the Patel lab[74, 78].

Conclusions

We have carried out a combined experimental and computational study of model 1:1 salt solvation in NMA, which was used as a model system representing the backbone of proteins. Corrected force-field parameters for polarizable and non-polarizable simulations were presented. A polarizable force-field based on the classical Drude oscillator is capable of reproducing energetics and geometries of the gas-phase clusters, and yields qualitative agreement with experimental data on the concentration-dependence of solvation enthalpies. To test the effect of the induced polarizability on the energetics of ion transport we studied a model narrow pore with the permeation pathway lined by backbone carbonyls. It was found that induced polarization has a dramatic impact on the computed Potentials of Mean Force.

It must be noted that the lack of comprehensive force-field validations [79, 80] may have significant impact on the computation of the thermodynamics of ion interactions with a protein binding site. In this paper we used a very well-studied membrane protein – gramicidin A (gA), where Li^+ binding to the channel was measured, as a testing ground for the parameters developed. The binding constants computed with polarizable force-field display excellent agreement with the reported data signifying role of induced polarization in Li+ permeation processes. Having only 3 e-, Li^+ is almost invisible in crystallographic studies of proteins. However, there are several reports detailing possible modes of binding for Li^+ to various biomolecular targets[81], including recent (2015) publication of the high-resolution crystal structure of Mycobacterium tuberculosis CysQ enzyme[82]. In most of the structures available to date Li^+ is coordinated by charged carboxylate groups or phosphate oxygens from the ligand and the direct comparisons to coordination mode by carbonyl oxygens is somewhat difficult. The *E. Coli* HU Beta-2 protein (PDB:4P3V) displays a coordination of Li+ by main chain carbonyl oxygen and water molecules. The coordination distance between carbonyl oxygen and bound ion is ~2.3 Å, which is consistent with results from simulations with polarizable force-fields. Further work will be required to understand modes of binding exhibited by Li^+ in a variety of protein binding sites with different chemical composition.

Notes and References

Useful discussions with Drs. Van Ngo, Chunfeng Zhao and Benoit Roux are acknowledged. This work was supported by the Natural Sciences and Engineering Research Council of Canada (NSERC) Discovery grant program (RGPIN 340946-07 to SN and RGPIN- 10174 to D.R.S) and a Resource Allocation Award from the Compute Canada (Westgrid). SN thanks an Alberta Innovates Technology Futures (AITF) New Faculty award. Experimental work at the Russian Academy of Sciences was supported by the Russian Foundation for Basic Research Grant (RFBR 13-03-12041).

1. F. T. Yu, V. M. Cangelosi, M. L. Zastrow, M. Tegoni, J. S. Plegaria, A. G. Tebo, C. S. Mocny, L. Ruckthong, H. Qayyum and V. L. Pecoraro, *Chem Rev*, 2014, 114, 3495-3578.
2. T. Dudev and C. Lim, *Chem Rev*, 2014, 114, 538-556.
3. H. B. Yu, T. W. Whitfield, E. Harder, G. Lamoureux, I. Vorobyov, V. M. Anisimov, A. D. MacKerell and B. Roux, *J Chem Theory Comput*, 2010, 6, 774-786.
4. K. M. Merz, *Accounts Chem Res*, 2014, 47, 2804-2811.
5. T. Heinisch, M. Pellizzoni, M. Durrenberger, C. E. Tinberg, V. Kohler, J. Klehr, D. Haussinger, D. Baker and T. R. Ward, *J Am Chem Soc*, 2015, DOI: 10.1021/jacs.5b06622.
6. C. Maffeo, S. Bhattacharya, J. Yoo, D. Wells and A. Aksimentiev, *Chem Rev*,

2012, 112, 6250-6284.
7. L. Borre and B. I. Kanner, *J Biol Chem*, 2001, 276, 40396-40401.
8. L. Borre, M. P. Kavanaugh and B. I. Kanner, *J Biol Chem*, 2002, 277, 13501-13507.
9. B. I. Kanner and E. Zomot, *Chem Rev*, 2008, 108, 1654-1668.
10. S. Stolzenberg, M. Quick, C. F. Zhao, K. Gotfryd, G. Khelashvili, U. Gether, C. J. Loland, J. A. Javitch, S. Noskov, H. Weinstein and L. Shi, *Journal of Biological Chemistry*, 2015, 290, 13992-14003.
11. H. K. Manji and R. H. Lenox, *Neuropsychopharmacol*, 1998, 19, 161-166.
12. E. Shorter, *Bipolar Disord*, 2009, 11, 4-9.
13. O. Boudker, R. M. Ryan, D. Yernool, K. Shimamoto and E. Gouaux, *Nature*, 2007, 445, 387-393.
14. R. W. Wheatley, D. H. Juers, B. B. Lev, R. E. Huber and S. Y. Noskov, *Phys Chem Chem Phys*, 2015, 17, 10899-10909.
15. T. Dudev, M. Devereux, M. Meuwly, C. Lim, J. P. Piquemal and N. Gresh, *J Comput Chem*, 2015, 36, 285-302.
16. S. Y. Noskov and B. Roux, *Journal of Molecular Biology*, 2008, 377, 804-818.
17. D. A. Caplan, J. O. Subbotina and S. Y. Noskov, *Biophys J*, 2008, 95, 4613-4621.
18. I. S. Joung and T. E. Cheatham, *J Phys Chem B*, 2008, 112, 9020-9041.
19. P. F. Li, L. F. Song and K. M. Merz, *J Chem Theory Comput*, 2015, 11, 1645-1657.
20. L. T. Costa, B. Sun, F. Jeschull and D. Brandell, *J Chem Phys*, 2015, 143.
21. H. Yu, S. Y. Noskov and B. Roux, *Proceedings of the National Academy of Sciences of the United States of America*, 2010, 107, 20329-20334.
22. A. Kolker, L. P. S. Safonova, A. N. Kinchin and G. A. Krestov, *J Solution Chem*, 1990, 19, 975-994.
23. A. M. Kolker, A. N. Kinchin and L. P. Safonova, *Thermochim Acta*, 1990, 169, 347-352.
24. L. P. Safonova, D. V. Sakharov, L. E. Shmukler and A. M. Kolker, *Phys Chem Chem Phys*, 2001, 3, 819-823.
25. G. I. Egorov and D. M. Makarov, *J Chem Thermodyn*, 2011, 43, 430-441.
26. N. G. Manin, A. Fini, A. N. Manin and G. L. Perlovich, *J Therm Anal Calorim*, 2007, 90, 147-152.
27. N. G. Manin, A. Fini and G. L. Perlovich, *J Therm Anal Calorim*, 2011, 104, 279-289.
28. L. P. Safonova, M. G. Kiselev and I. V. Fedorova, *Pure Appl Chem*, 2013, 85, 225-236.
29. L. P. Safonova, E. V. Svetsova and M. G. Kiselev, *J Solution Chem*, 2005, 34, 529-536.
30. M.S.Gordon and M.W.Schmidt, in *Theory and Applications of Computational Chemistry: the first forty years*, eds. C.E.Dykstra, G.Frenking, K.S.Kim and G.E.Scuseria, Elsevier, Amsterdam, 2005.
31. V. B. Parker, *Thermal properties of aqueous uni-univalent electrolytes.*, Nat. Bur. Stand. (USA), 1965.
32. D. Cubicciotti, *J Chem Phys*, 1959, 31, 1646-1651.
33. D. Cubicciotti, *J Chem Phys*, 1961, 34, 2189-&.
34. J. P. Perdew, K. Burke and M. Ernzerhof, *Phys Rev Lett*, 1996, 77, 3865-3868.
35. A. D. Becke, *Phys Rev A*, 1988, 38, 3098-3100.
36. C. T. Lee, W. T. Yang and R. G. Parr, *Phys Rev B*, 1988, 37, 785-789.
37. B. Miehlich, A. Savin, H. Stoll and H. Preuss, *Chem Phys Lett*, 1989, 157, 200-206.
38. J. P. Perdew, K. Burke and Y. Wang, *Phys Rev B*, 1996, 54, 16533-16539.
39. J. M. Tao, J. P. Perdew, V. N. Staroverov and G. E. Scuseria, *Phys Rev Lett*, 2003, 91.
40. A. D. Becke, *J Chem Phys*, 1993, 98, 5648-5652.
41. S. H. Vosko, L. Wilk and M. Nusair, *Can J Phys*, 1980, 58, 1200-1211.
42. A. D. Boese and J. M. L. Martin, *J Chem Phys*, 2004, 121, 3405-3416.
43. Y. Zhao, N. E. Schultz and D. G. Truhlar, *J Chem Theory Comput*, 2006, 2, 364-382.
44. R. Krishnan, J. S. Binkley, R. Seeger and J. A. Pople, *J Chem Phys*, 1980, 72, 650-654.
45. T. Clark, J. Chandrasekhar, G. W. Spitznagel and P. V. Schleyer, *J Comput Chem*, 1983, 4, 294-301.
46. M. J. T. Frisch, G. W.; Schlegel, H. B.; Scuseria, G. E.; Robb, M. A.; Cheeseman, J. R.; Scalmani, G.; Barone, V.; Mennucci, B.; Petersson, G. A.; Nakatsuji, H.; Caricato, M.; Li, X.; Hratchian, H. P.; Izmaylov, A. F.; Bloino, J.; Zheng, G.; Sonnenberg, J. L.; Hada, M.; Ehara, M.; Toyota, K.; Fukuda, R.; Hasegawa, J.; Ishida, M.; Nakajima, T.; Honda, Y.; Kitao, O.; Nakai, H.; Vreven, T.; Montgomery, J. A., Jr.; Peralta, J. E.; Ogliaro, F.; Bearpark, M.; Heyd, J. J.; Brothers, E.; Kudin, K. N.; Staroverov, V. N.; Kobayashi, R.; Normand, J.; Raghavachari, K.; Rendell, A.; Burant, J. C.; Iyengar, S. S.; Tomasi, J.; Cossi, M.; Rega, N.; Millam, J. M.; Klene, M.; Knox, J. E.; Cross, J. B.; Bakken, V.; Adamo, C.; Jaramillo, J.; Gomperts, R.; Stratmann, R. E.; Yazyev, O.; Austin, A. J.; Cammi, R.; Pomelli, C.; Ochterski, J. W.; Martin, R. L.; Morokuma, K.; Zakrzewski, V. G.; Voth, G. A.; Salvador, P.; Dannenberg, J. J.; Dapprich, S.; Daniels, A. D.; Farkas, Ö.; Foresman, J. B.; Ortiz, J. V.; Cioslowski, J.; Fox, D. J., Gaussian, Inc., Wallingford CT, 2009., 2009.
47. S. Simon, M. Duran and J. J. Dannenberg, *J Chem Phys*, 1996, 105, 11024-11031.
48. D. Rappoport and F. Furche, *J Chem Phys*, 2010, 133.
49. R. M. Noyes, *Journal of the American Chemical Society*, 1962, 84, 513-&.
50. C. E. Klots, *J Phys Chem-Us*, 1981, 85, 3585-3588.
51. Y. Marcus, *J Chem Soc Faraday T*, 1991, 87, 2995-2999.
52. L. E. Townsley, W. A. Tucker, S. Sham and J. F. Hinton, *Biochemistry-Us*, 2001, 40, 11676-11686.
53. T. W. Allen, O. S. Andersen and B. Roux, *Journal of the American Chemical Society*, 2003, 125, 9868-9877.
54. T. W. Allen, O. S. Andersen and B. Roux, *Proceedings of the National Academy of Sciences of the United States of America*, 2004, 101, 117-122.
55. H. Ohtaki, N. Katayama, K. Ozutsumi and T. Radnai, *J Mol Liq*, 2000, 88, 109-120.
56. H. Ohtaki and H. Wada, *J Solution Chem*, 1985, 14, 209-219.
57. P. J. Cheek, M. A. Gallardojimenez and T. H. Lilley, *J Chem Soc Farad T 1*, 1988, 84, 3435-3443.
58. M. A. Gallardojimenez and T. H. Lilley, *J Chem Soc Farad T 1*, 1989, 85, 2909-2915.
59. R. J. Blint, *J Electrochem Soc*, 1995, 142, 696-702.
60. H. Li, Ngo, V. A., Da Silva, M. C., Callahan, K. M., Salahub, D. R., Roux, B., & Noskov, S. Y., *J Phys Chem B*, 2015, 119 9401–9416.
61. B. Lev, B. Roux and S. Y. Noskov, *J Chem Theory Comput*, 2013, 9, 4165-4175.
62. M. D. Tissandier, K. A. Cowen, W. Y. Feng, E. Gundlach, M. H. Cohen, A. D. Earhart, T. R. Tuttle and J. V. Coe, *J Phys Chem A*, 1998, 102, 9308-9308.
63. S. B. Nielsen, M. Masella and P. Kebarle, *J Phys Chem A*, 1999, 103, 9891-9898.
64. C. P. Kelly, C. J. Cramer and D. G. Truhlar, *J Phys Chem B*, 2006, 110, 16066-16081.
65. V. Ngo, M. C. da Silva, M. Kubillus, H. Li, B. Roux, M. Elstner, Q. Cui, D. R. Salahub and S. Y. Noskov, *J Chem Theory Comput*, 2015, 11, 4992-5001.
66. B. Lin, P. E. M. Lopes, B. Roux and A. D. MacKerell, *J Chem Phys*, 2013, 139.
67. P. E. M. Lopes, J. Huang, J. Shim, Y. Luo, H. Li, B. Roux and A. D. MacKerell, *J Chem Theory Comput*, 2013, 9, 5430-5449.
68. S. Patel and C. L. Brooks, *Mol Simulat*, 2006, 32, 231-249.
69. N. Gresh, G. A. Cisneros, T. A. Darden and J. P. Piquemal, *J Chem Theory Comput*, 2007, 3, 1960-1986.
70. N. Gresh, J. P. Piquemal and M. Krauss, *J Comput Chem*, 2005, 26, 1113-1130.
71. Y. P. Zeng, C. F. Wang, X. B. Zhang and S. G. Ju, *Chem Phys*, 2014, 433, 89-97.
72. J. A. Dani and D. G. Levitt, *Biophys J*, 1981, 35, 485-499.
73. D. D. Busath, *Annu Rev Physiol*, 1993, 55, 473-501.
74. S. Patel, J. E. Davis and B. A. Bauer, *J Am Chem Soc*, 2009, 131, 13890-13891.
75. T. W. Allen, O. S. Andersen and B. Roux, *Biophys J*, 2006, 90, 3447-3468.
76. D. Asthagiri, P. D. Dixit, S. Merchant, M. E. Paulaitis, L. R. Pratt, S. B. Rempe and S. Varma, *Chem Phys Lett*, 2010, 485, 1-7.
77. R. R. Ketchem, B. Roux and T. A. Cross, *Structure*, 1997, 5, 1655-1669.
78. J. E. Davis and S. Patel, *J Phys Chem B*, 2009, 113, 9183-9196.
79. M. P. Jacobson, G. A. Kaminski, R. A. Friesner and C. S. Rapp, *The Journal of Physical Chemistry B*, 2002, 106, 11673-11680.
80. S. L. Peck, *Trends in Ecology & Evolution*, 2004, 19, 530-534.
81. V. Villeret, S. H. Huang, H. J. Fromm and W. N. Lipscomb, *Proceedings of the National Academy of Sciences of the United States of America*, 1995, 92, 8916-8920.
82. A. I. Erikson, R. D. Sarsam and A. J. Fisher, *Biochemistry-Us*, 2015, DOI: 10.1021/acs.biochem.5b01000.